MITC9 shell elements based on refined theories for the analysis of isotropic cylindrical structures

M. Cinefra[1,2] *, C. Chinosi[3†], L. Della Croce[4‡],
(1) Department of Aeronautics and Space Engineering,
Politecnico di Torino, Torino, Italy.
(2) CRP H. Tudor, Esch-sur-Alzette, Luxembourg.
(3) Department of Sciences and Advanced Technologies,
Universita' del Piemonte Orientale, Alessandria, Italy
(4) Department of Mathematics, Università di Pavia, Pavia, Italy.

Submitted to: Mechanics of Advanced Materials and Structures

Author for correspondence:
Maria Cinefra, PhD student,
Department of Aeronautic and Space Engineering,
Politecnico di Torino,
Corso Duca degli Abruzzi 24,
10129 Torino, Italy,
tel: +39 011 090 6869,
e-mail: maria.cinefra@polito.it

*PhD student, e-mail: maria.cinefra@polito.it
†Professor of Mathematics, e-mail: claudia.chinosi@mfn.unipmn.it
‡Professor of Mathematics, e-mail: lucia.dellacroce@unipv.it

keywords: Shell elements; membrane and shear locking; Mixed Interpolation of Tensorial Compomenets; refined theories; static analysis.

Abstract

In this work a nine-nodes shell finite element, formulated in the framework of Carrera's Unified Formulation (CUF), is presented. The exact geometry of cylindrical shells is considered. The Mixed Interpolation of Tensorial Components (MITC) technique is applied to the element in order to overcome shear and membrane locking phenomenon. High-order equivalent single layer theories contained in the CUF are used to perform the analysis of shell structures. Benchmark solutions from the open literature are taken to validate the obtained results. The mixed-interpolated shell finite element shows good properties of convergence and robustness by increasing the number of used elements and the order of expansion of displacements in the thickness direction.

1 Introduction

The efficient load-carrying capabilities of shell structures make them very useful in a variety of engineering applications. The continuous development of new structural materials leads to ever increasingly complex structural designs that require careful analysis. Although analytical techniques are very important, the use of numerical methods to solve shell mathematical models of complex structures has become an essential ingredient in the design process. The finite element method has been the fundamental numerical procedure for the analysis of the shells.
The most common mathematical models used to describe shell structures may be classified in two classes according to different physical assumptions. The Koiter model [1] is based on the Kirchhoff hypothesis. The Naghdi model [2] is based on the Reissner-Mindlin assumptions that take into account the transverse shear deformation. It is known that when a finite element method is used to discretize a physical model, the phenomenon of numerical *locking* may arise from hidden constrains that are not well represented in the finite element approximation. In the Naghdi model both transverse shear and membrane constraints appear as the shell thickness becomes very small, thus the locking may arise. A locking phenomenon that is particularly well understood is the *shear locking* of plates [3]. In shells the shear locking is still present, but another and more severe type of locking, referred to as *membrane locking*, appears [4][5]. The most common approaches proposed to overcome the locking phenomenon are the use of standard displacement formulation with higher-order elements (see [6],[7]). The numerical results show that high-order elements are able to contrast locking for the shell problem in its displacement formulation. However, in the case of very small thickness and when the element is not of degree as high as needed, the numerical solution exhibits a loss in the rate of convergence [5]. Another remedy for the locking is the use of several techniques of reduced-selective integration (see [8],[9]) but they fail because the additional degrees of freedom at the center of the element produce spurious modes. Finally, in scientific literature it is possible to find many examples of modified variational forms to overcome the locking problem (see [10]-[15]) and they provide good results.

In this paper we propose a new shell finite element based on the refined Equivalent Single Layer (ESL) theories contained in the Carrera's Unified Formulation [16]-[20]. The classical models, such as Koiter and Naghdi models, can be also obtained from an ESL theory with linear expansion of displacements along the thickness by applying penalty techniques. In the wake of Bathe et al. [21]-[24], the Mixed Interpolation of Tensorial Components (MITC) method has been extended to variable kinematic models for the case of shell elements with nine nodes. The aim of the work is to prove that the extension of MITC to high-order ESL shell elements is

feasible and to show that such an extension is numerically efficient. The performance of the new element is tested by solving benchmark problems involving very thin shells. The results show both the properties of convergence and robustness.
The outline of the paper is the following. In Section 2 we recall the main features of the Unified Formulation. In Section 3 the geometry of cylindrical shells is described. In Section 4 the MITC technique is extended to Unified Formulation. Section 5 deals with the governing equations. In Section 6 we report several numerical results. Section 7 contains the conclusions that can be drawn from this work.

2 Variable Kinematic model via Carrera Unified Formulation

Carrera Unified Formulation (CUF) is a technique which handles a large variety of bi-dimensional models in a unified manner [16]. According to CUF, the governing equations are written in terms of a few fundamental nuclei which do not formally depend on the order of expansion N used in the z direction. The application of a two-dimensional method for shells permits to express the unknown variables as a set of thickness functions depending only on the thickness coordinate z and the corresponding variables depending on the in plane coordinates α and β. So that, a generic variable, for instance the displacement $u(\alpha, \beta, z)$, and its variation $\delta u(\alpha, \beta, z)$ are written according to the following general expansion:

$$\boldsymbol{u}(\alpha, \beta, z) = F_s(z)\boldsymbol{u}_s(\alpha, \beta), \qquad \delta\boldsymbol{u}(\alpha, \beta, z) = F_\tau(z)\delta\boldsymbol{u}_\tau(\alpha, \beta), \qquad \text{with} \quad \tau, s = 0, ..., N \tag{1}$$

Bold letters denote arrays and the summing convention with repeated indexes τ and s is assumed. The order of expansion N goes from first to higher-order values. A Taylor expansion is employed as thickness function $F(z)$:

$$\boldsymbol{u} = F_0\,\boldsymbol{u}_0 + F_1\,\boldsymbol{u}_1 + \ldots + F_N\,\boldsymbol{u}_N = F_\tau\,\boldsymbol{u}_\tau \;\; with \;\; \tau = 0, 1, \ldots, N \tag{2}$$

$$F_0 = z^0 = 1, \;\; F_1 = z^1 = z, \;\; \ldots, \;\; F_N = z^N \tag{3}$$

It is possible to obtain the Naghdi model [2] from a theory with first order of expansion, by considering a constant transverse displacement through the thickness. An appropriate application of penalty techniques to shear correction factor leads to Koiter [1].

3 Geometry of a thin shell

Let R^3 be the usual euclidean space (O, x, y, z) and let Ω be an open bounded subset of R^2 with closure $\bar{\Omega}$. Let (ξ_1, ξ_2) denote a generic point of the set $\bar{\Omega}$. Let $\boldsymbol{\Phi}$ be a smooth one-to-one mapping of $\bar{\Omega}$ into R^3. The middle surface $\bar{S}$ of the shell (see Figure 1) is the image in R^3 of the set $\bar{\Omega}$ through the mapping $\boldsymbol{\Phi}$:

$$\boldsymbol{\Phi} = (\Phi_1, \Phi_2, \Phi_3) : \;\; \bar{\Omega} \subset R^2 \rightarrow \bar{S} \subset R^3 \tag{4}$$

Thus we have $\bar{S} = \boldsymbol{\Phi}(\bar{\Omega})$. Let us set $\boldsymbol{a}_\alpha = \boldsymbol{\Phi}_{,\alpha} = \partial\boldsymbol{\Phi}/\partial\xi_\alpha$. The vectors $\boldsymbol{a}_1, \boldsymbol{a}_2$ are linearly independent at each point of $\bar{\Omega}$ and define the tangent plane to the midsurface $\bar{S}$ at each point $\boldsymbol{\Phi}(\xi_1, \xi_2)$. Let $\boldsymbol{a}_3$ be the unit vector normal to the tangent plane. The set of vectors $\boldsymbol{a}_1, \boldsymbol{a}_2, \boldsymbol{a}_3$ define the covariant basis at the point $\boldsymbol{\Phi}(\xi_1, \xi_2)$. The first fundamental form is $a_{\alpha\beta} = \boldsymbol{a}_\alpha \cdot \boldsymbol{a}_\beta$, with $a = \det(a_{\alpha\beta})$. Denoting by $a^{\alpha\beta}$ the components of the inverse matrix to $(a_{\alpha\beta})$, we introduce

the contravariant basis $\boldsymbol{a}^\alpha = a^{\alpha\beta}\boldsymbol{a}_\beta$ and we set $\boldsymbol{a}^3 = \boldsymbol{a}_3$. The second fundamental form is $b_{\alpha\beta} = \boldsymbol{a}_3 \cdot \boldsymbol{a}_{\alpha,\beta} = \boldsymbol{a}_3 \cdot \boldsymbol{a}_{\beta,\alpha}$ and the following relation holds:

$$a^{\alpha\beta} \cdot b_{\beta\gamma} = b^\alpha_\gamma \tag{5}$$

Let us consider a cylindrical shell. In a system of Cartesian coordinates (O, x, y, z), the region occupied by the midsurface of the shell is:

$$S = \{(x, y, z) \in R^3 : \ -L/2 < x < L/2, \ \ y^2 + z^2 = R^2\} \tag{6}$$

where L and R are the length and the radius of the shell, respectively. Let us take a curvilinear coordinate system $(\alpha, \beta, z) = (\xi_1, \xi_2, z)$ placed at the center of the upper part of the midsurface. The 3D medium corresponding to the shell is defined by the 3D chart given by:

$$\boldsymbol{\Phi}(\alpha, \beta, z) = \boldsymbol{\phi}(\alpha, \beta) + z\boldsymbol{a}_3(\alpha, \beta) \tag{7}$$

Then, the midsurface S of the cylindrical shell is described by the following 2D chart:

$$\begin{cases} \phi_1(\alpha, \beta) = \alpha \\ \phi_2(\alpha, \beta) = R\sin(\beta/R) \\ \phi_3(\alpha, \beta) = R\cos(\beta/R) \end{cases} \tag{8}$$

With such choices, the region $\Omega \subset R^2$ corresponding to the midsurface S is the rectangle:

$$\Omega = \{(\alpha, \beta) : \ -L/2 < \alpha < L/2, \ \ -R\pi < \beta < R\pi\} \tag{9}$$

In the Unified Formulation the unknowns are the covariant components of the displacement $u_\tau(\alpha, \beta)$, $v_\tau(\alpha, \beta)$ and $w_\tau(\alpha, \beta)$, for $\tau = 0, 1, ..., N$. The strain-displacement relations are given by the linear part of the *3D Green Lagrange strain tensor* and they are:

$$\begin{aligned} \varepsilon_{\alpha\alpha} &= F_\tau u_{\tau,\alpha} \\ \varepsilon_{\beta\beta} &= F_\tau \Big[\big(1 + \frac{z}{R}\big) \frac{w_\tau}{R} + \big(1 + \frac{z}{R}\big) v_{\tau,\beta} \Big] \\ \varepsilon_{\alpha\beta} &= F_\tau \Big[u_{\tau,\beta} + \big(1 + \frac{z}{R}\big) v_{\tau,\alpha} \Big] \\ \varepsilon_{\alpha z} &= w_{\tau,\alpha} F_\tau + u_\tau F_{\tau,z} \\ \varepsilon_{\beta z} &= F_\tau \Big[w_{\tau,\beta} - \frac{v_\tau}{R} \Big] + F_{\tau,z} \Big[\big(1 + \frac{z}{R}\big) v_\tau \Big] \\ \varepsilon_{zz} &= w_\tau F_{\tau,z} \end{aligned} \tag{10}$$

where the previous geometrical assumptions are applied. For more details about mathematical passages, the reader can refer to [25]. These geometrical relations can be expressed in matrix form as:

$$\begin{aligned} \boldsymbol{\varepsilon}_p &= (\boldsymbol{D}_p + \boldsymbol{A}_p)\boldsymbol{u} \\ \boldsymbol{\varepsilon}_n &= (\boldsymbol{D}_{n\Omega} + \boldsymbol{D}_{nz} - \boldsymbol{A}_n)\boldsymbol{u} \end{aligned} \tag{11}$$

where subscripts (p) and (n) indicate in-plane and normal components, respectively, and the differential operators are defined as follows:

$$\boldsymbol{D}_p = \begin{bmatrix} \partial_\alpha & 0 & 0 \\ 0 & H\partial_\beta & 0 \\ \partial_\beta & H\partial_\alpha & 0 \end{bmatrix} \quad , \quad \boldsymbol{D}_{n\Omega} = \begin{bmatrix} 0 & 0 & \partial_\alpha \\ 0 & 0 & \partial_\beta \\ 0 & 0 & 0 \end{bmatrix} \quad , \quad \boldsymbol{D}_{nz} = \partial_z \cdot \boldsymbol{A}_{nz} = \partial_z \begin{bmatrix} 1 & 0 & 0 \\ 0 & H & 0 \\ 0 & 0 & 1 \end{bmatrix} \quad , \tag{12}$$

$$\boldsymbol{A}_p = \begin{bmatrix} 0 & 0 & 0 \\ 0 & 0 & \frac{1}{R}H \\ 0 & 0 & 0 \end{bmatrix} \, , \boldsymbol{A}_n = \begin{bmatrix} 0 & 0 & 0 \\ 0 & \frac{1}{R} & 0 \\ 0 & 0 & 0 \end{bmatrix} \quad . \tag{13}$$

and $H = (1 + \frac{z}{R})$.

4 CUF extended to MITC9 shell finite element

Considering the (covariant) components of the strain tensor in the local coordinate system (ξ, η, z), the MITC shell elements are formulated by using - instead of the strain components directly computed form the displacements - an interpolation of these strain components within each element using a specific interpolation strategy for each component. The corresponding interpolation points - called the *tying points* are shown in figure 2 for the MITC9 shell element.

The interpolating functions are arranged in the following arrays:

$$\begin{aligned} N_{m1} &= [N_{A1}, N_{B1}, N_{C1}, N_{D1}, N_{E1}, N_{F1}] \\ N_{m2} &= [N_{A2}, N_{B2}, N_{C2}, N_{D2}, N_{E2}, N_{F2}] \\ N_{m3} &= [N_P, N_Q, N_R, N_S] \end{aligned} \tag{14}$$

For convenience, from this point on we indicate with the subscripts $m1$, $m2$ and $m3$ the quantities calculated in the points $(A1, B1, C1, D1, E1, F1)$, $(A2, B2, C2, D2, E2, F2)$ and (P, Q, R, S), respectively.

According to MITC method, the strains components are interpolated on tying points as follows:

$$\begin{aligned} \boldsymbol{\varepsilon}_p &= \begin{bmatrix} \varepsilon_{11} \\ \varepsilon_{22} \\ \varepsilon_{12} \end{bmatrix} = \begin{bmatrix} N_{m1} & 0 & 0 \\ 0 & N_{m2} & 0 \\ 0 & 0 & N_{m3} \end{bmatrix} \begin{bmatrix} \varepsilon_{11_{m1}} \\ \varepsilon_{22_{m2}} \\ \varepsilon_{12_{m3}} \end{bmatrix} = [\boldsymbol{N1}] \begin{bmatrix} \varepsilon_{11_{m1}} \\ \varepsilon_{22_{m2}} \\ \varepsilon_{12_{m3}} \end{bmatrix} \\ \boldsymbol{\varepsilon}_n &= \begin{bmatrix} \varepsilon_{13} \\ \varepsilon_{23} \\ \varepsilon_{33} \end{bmatrix} = \begin{bmatrix} N_{m1} & 0 & 0 \\ 0 & N_{m2} & 0 \\ 0 & 0 & 1 \end{bmatrix} \begin{bmatrix} \varepsilon_{13_{m1}} \\ \varepsilon_{23_{m2}} \\ \varepsilon_{33} \end{bmatrix} = [\boldsymbol{N2}] \begin{bmatrix} \varepsilon_{13_{m1}} \\ \varepsilon_{23_{m2}} \\ \varepsilon_{33} \end{bmatrix} \end{aligned} \tag{15}$$

where the matrixes $\boldsymbol{N1}$ and $\boldsymbol{N2}$ are introduced.

Applying the finite element method (FEM), the unknown displacements are interpolated on the nodes of the finite element by means of the Lagrangian shape functions N_i (for $i = 1, ...9$):

$$\boldsymbol{u} = F_\tau N_i \boldsymbol{q}_{\tau_i} \tag{16}$$

where $\boldsymbol{q}_{\tau_i}$ are the nodal displacements and the Unified Formulation is applied. Substituting in eq.s (11) the geometrical relations become:

$$\begin{aligned}\boldsymbol{\varepsilon}_p =& F_\tau(\boldsymbol{D}_p + \boldsymbol{A}_p)(N_i\boldsymbol{I})\boldsymbol{q}_{\tau_i} \\ \boldsymbol{\varepsilon}_n =& F_\tau(\boldsymbol{D}_{n\Omega} - \boldsymbol{A}_n)(N_i\boldsymbol{I})\boldsymbol{q}_{\tau_i} + F_{\tau,z}\boldsymbol{A}_{nz}(N_i\boldsymbol{I})\boldsymbol{q}_{\tau_i}\end{aligned} \tag{17}$$

where $\boldsymbol{I}$ is a 3×3 identity matrix.

If the MITC technique is applied to the strains, the geometrical relations are re-written in the following manner:

$$\begin{aligned}\boldsymbol{\varepsilon}^\tau_{p_{im}} =& F_\tau[\boldsymbol{C}_{3_{im}}]\boldsymbol{q}_{\tau_i} \\ \boldsymbol{\varepsilon}^\tau_{n_{im}} =& F_\tau[\boldsymbol{C}_{1_{im}}]\boldsymbol{q}_{\tau_i} + F_{\tau,z}[\boldsymbol{C}_{2_{im}}]\boldsymbol{q}_{\tau_i}\end{aligned} \tag{18}$$

where the introduced matrixes are:

$$\begin{aligned}[\boldsymbol{C}_{1_{im}}] =& [\boldsymbol{N2}]\begin{bmatrix}[(\boldsymbol{D}_{n\Omega} - \boldsymbol{A}_n)(N_i\boldsymbol{I})]_{m1}(1,:) \\ [(\boldsymbol{D}_{n\Omega} - \boldsymbol{A}_n)(N_i\boldsymbol{I})]_{m2}(2,:) \\ [(\boldsymbol{D}_{n\Omega} - \boldsymbol{A}_n)(N_i\boldsymbol{I})](3,:)\end{bmatrix} \\ [\boldsymbol{C}_{2_{im}}] =& [\boldsymbol{N2}]\begin{bmatrix}[\boldsymbol{A}_{nz}(N_i\boldsymbol{I})]_{m1}(1,:) \\ [\boldsymbol{A}_{nz}(N_i\boldsymbol{I})]_{m2}(2,:) \\ [\boldsymbol{A}_{nz}(N_i\boldsymbol{I})](3,:)\end{bmatrix} \\ [\boldsymbol{C}_{3_{im}}] =& [\boldsymbol{N1}]\begin{bmatrix}[(\boldsymbol{D}_p + \boldsymbol{A}_p)(N_i\boldsymbol{I})]_{m1}(1,:) \\ [(\boldsymbol{D}_p + \boldsymbol{A}_p)(N_i\boldsymbol{I})]_{m2}(2,:) \\ [(\boldsymbol{D}_p + \boldsymbol{A}_p)(N_i\boldsymbol{I})]_{m3}(3,:)\end{bmatrix}\end{aligned} \tag{19}$$

$(1,:)$, $(2,:)$ and $(3,:)$ respectively indicate that the first, second or third line of the relative matrix is considered.

5 Governing equations

This section presents the derivation of the governing equations based on the *Principle of Virtual Displacements* (PVD) in case of shell structures subjected to mechanical load. CUF permits to obtain the so-called *fundamental nuclei*, which are simple matrices representing the basic elements from which the stiffness matrix of the whole structure can be computed.

The PVD for a shell reads:

$$\int_V (\delta\boldsymbol{\varepsilon}^T_{pG}\boldsymbol{\sigma}_{pC} + \delta\boldsymbol{\varepsilon}^T_{nG}\boldsymbol{\sigma}_{nC})dV = \delta L_e, \tag{20}$$

where V is the volume of the shell and T indicate the transpose of a vector. The first member of the equation represents the variation of internal work δL_{int} and δL_e is the external work. G

means geometrical relations and C constitutive relations.
The first step to derive the fundamental nuclei is the substitution of *constitutive equations* (C) in the variational statement PVD, which are:

$$\begin{aligned} \boldsymbol{\sigma}_{pC} &= \boldsymbol{\sigma}^s_{p_{jn}} = \boldsymbol{C}_{pp}\, \boldsymbol{\varepsilon}^s_{p_{jn}} + \boldsymbol{C}_{pn}\, \boldsymbol{\varepsilon}^s_{n_{jn}} \\ \boldsymbol{\sigma}_{nC} &= \boldsymbol{\sigma}^s_{n_{jn}} = \boldsymbol{C}_{np}\, \boldsymbol{\varepsilon}^s_{p_{jn}} + \boldsymbol{C}_{nn}\, \boldsymbol{\varepsilon}^s_{n_{jn}} \end{aligned} \tag{21}$$

with

$$\begin{aligned} \boldsymbol{C}_{pp} &= \begin{bmatrix} C_{11} & C_{12} & C_{16} \\ C_{12} & C_{22} & C_{26} \\ C_{16} & C_{26} & C_{66} \end{bmatrix} \qquad \boldsymbol{C}_{pn} = \begin{bmatrix} 0 & 0 & C_{13} \\ 0 & 0 & C_{23} \\ 0 & 0 & C_{36} \end{bmatrix} \\ \boldsymbol{C}_{np} &= \begin{bmatrix} 0 & 0 & 0 \\ 0 & 0 & 0 \\ C_{13} & C_{23} & C_{36} \end{bmatrix} \qquad \boldsymbol{C}_{nn} = \begin{bmatrix} C_{55} & C_{45} & 0 \\ C_{45} & C_{44} & 0 \\ 0 & 0 & C_{33} \end{bmatrix} \end{aligned} \tag{22}$$

Then, one substitutes the geometrical relations (18) and the Unified formulation (1) in eq.(20) and obtains the governing equation system:

$$\delta \boldsymbol{u}_\tau^{k^T} : \qquad \boldsymbol{K}^{\tau s}_{uu}\, \boldsymbol{u}_s \;=\; \boldsymbol{P}_{u\tau}\ , \tag{23}$$

where $\boldsymbol{K}^{\tau s}_{uu}$ is the fundamental nucleo of the stiffness array and it is expanded according to the indexes τ and s in order to obtain the matrix for the whole shell.
The boundary conditions of Neumann type state:

$$\boldsymbol{\Pi}^{\tau s}_{uu}\, \boldsymbol{u}_s \;=\; \boldsymbol{\Pi}^{\tau s}_{uu}\, \bar{\boldsymbol{u}}_s \tag{24}$$

The explicit form of fundamental nucleus is the following:

$$\begin{aligned} K^{\tau sij}_{11} =& C_{55} N_{i_{m1}} \lhd N_{m1} N_{n1} \rhd_\Omega N_{j_{n1}} \lhd F_{\tau,_z} F_{s,_z} \rhd_A + C_{11} N_{i,\alpha_{m1}} \lhd N_{m1} N_{n1} \rhd_\Omega N_{j,\alpha_{n1}} \lhd F_\tau F_s \rhd_A + \\ & C_{16} N_{i,\beta_{m3}} \lhd N_{m3} N_{n1} \rhd_\Omega N_{j,\alpha_{n1}} \lhd F_\tau F_s \rhd_A + C_{16} N_{i,\alpha_{m1}} \lhd N_{m1} N_{n3} \rhd_\Omega N_{j,\beta_{n3}} \lhd F_\tau F_s \rhd_A + \\ & C_{66} N_{i,\beta_{m3}} \lhd N_{m3} N_{n3} \rhd_\Omega N_{j,\beta_{n3}} \lhd F_\tau F_s \rhd_A \end{aligned}$$

$$\begin{aligned} K^{\tau sij}_{12} =& -C_{45} \frac{1}{R} N_{i_{m1}} \lhd N_{m1} N_{n2} \rhd_\Omega N_{j_{n2}} \lhd F_{\tau,_z} F_s \rhd_A + C_{45} N_{i_{m1}} \lhd N_{m1} N_{n2} \rhd_\Omega N_{j_{n2}} \lhd H F_{\tau,_z} F_{s,_z} \rhd_A + \\ & C_{12} N_{i,\alpha_{m1}} \lhd N_{m1} N_{n2} \rhd_\Omega N_{j,\beta_{n2}} \lhd H F_\tau F_s \rhd_A + C_{16} N_{i,\alpha_{m1}} \lhd N_{m1} N_{n3} \rhd_\Omega N_{j,\alpha_{n3}} \lhd H F_\tau F_s \rhd_A + \\ & C_{26} N_{i,\beta_{m3}} \lhd N_{m3} N_{n2} \rhd_\Omega N_{j,\beta_{n2}} \lhd H F_\tau F_s \rhd_A + C_{66} N_{i,\beta_{m3}} \lhd N_{m3} N_{n3} \rhd_\Omega N_{j,\alpha_{n3}} \lhd H F_\tau F_s \rhd_A \end{aligned}$$

$$\begin{aligned} K^{\tau sij}_{13} =& C_{13} N_{i,\alpha_{m1}} \lhd N_{m1} N_j \rhd_\Omega \lhd F_\tau F_{s,_z} \rhd_A + C_{36} N_{i,\beta_{m3}} \lhd N_{m3} N_j \rhd_\Omega \lhd F_\tau F_{s,_z} \rhd_A + \\ & C_{12} \frac{1}{R} N_{i,\alpha_{m1}} \lhd N_{m1} N_{n2} \rhd_\Omega N_{j_{n2}} \lhd H F_\tau F_s \rhd_A + C_{26} \frac{1}{R} N_{i,\beta_{m3}} \lhd N_{m3} N_{n2} \rhd_\Omega N_{j_{n2}} \lhd H F_\tau F_s \rhd_A + \\ & C_{55} N_{i_{m1}} \lhd N_{m1} N_{n1} \rhd_\Omega N_{j,\alpha_{n1}} \lhd F_{\tau,_z} F_s \rhd_A + C_{45} N_{i_{m1}} \lhd N_{m1} N_{n2} \rhd_\Omega N_{j,\beta_{n2}} \lhd F_{\tau,_z} F_s \rhd_A \end{aligned} \tag{25}$$

$$
\begin{aligned}
K_{21}^{\tau sij} =& - C_{45}\frac{1}{R}N_{i_{m2}} \lhd N_{m2}N_{n1} \rhd_\Omega N_{j_{n1}} \lhd F_\tau F_{s_{,z}} \rhd_A + C_{45}N_{i_{m2}} \lhd N_{m2}N_{n1} \rhd_\Omega N_{j_{n1}} \lhd HF_{\tau_{,z}}F_{s_{,z}} \rhd_A + \\
& C_{12}N_{i,\beta_{m2}} \lhd N_{m2}N_{n1} \rhd_\Omega N_{j,\alpha_{n1}} \lhd HF_\tau F_s \rhd_A + C_{16}N_{i,\alpha_{m3}} \lhd N_{m3}N_{n1} \rhd_\Omega N_{j,\alpha_{n1}} \lhd HF_\tau F_s \rhd_A + \\
& C_{26}N_{i,\beta_{m2}} \lhd N_{m2}N_{n3} \rhd_\Omega N_{j,\beta_{n3}} \lhd HF_\tau F_s \rhd_A + C_{66}N_{i,\alpha_{m3}} \lhd N_{m3}N_{n3} \rhd_\Omega N_{j,\beta_{n3}} \lhd HF_\tau F_s \rhd_A \\
\\
K_{22}^{\tau sij} =& C_{22}N_{i,\beta_{m2}} \lhd N_{m2}N_{n2} \rhd_\Omega N_{j,\beta_{n2}} \lhd H^2F_\tau F_s \rhd_A + C_{26}N_{i,\beta_{m2}} \lhd N_{m2}N_{n3} \rhd_\Omega N_{j,\alpha_{n3}} \lhd H^2F_\tau F_s \rhd_A \\
& C_{26}N_{i,\alpha_{m3}} \lhd N_{m3}N_{n2} \rhd_\Omega N_{j,\beta_{n2}} \lhd H^2F_\tau F_s \rhd_A + C_{66}N_{i,\alpha_{m3}} \lhd N_{m3}N_{n3} \rhd_\Omega N_{j,\alpha_{n3}} \lhd H^2F_\tau F_s \rhd_A + \\
& C_{44}\frac{1}{R^2}N_{i_{m2}} \lhd N_{m2}N_{n2} \rhd_\Omega N_{j_{n2}} \lhd F_\tau F_s \rhd_A - C_{44}\frac{1}{R}N_{i_{m2}} \lhd N_{m2}N_{n2} \rhd_\Omega N_{j_{n2}} \lhd HF_\tau F_{s_{,z}} \rhd_A + \\
& - C_{44}\frac{1}{R}N_{i_{m2}} \lhd N_{m2}N_{n2} \rhd_\Omega N_{j_{n2}} \lhd HF_{\tau_{,z}}F_s \rhd_A + C_{44}N_{i_{m2}} \lhd N_{m2}N_{n2} \rhd_\Omega N_{j_{n2}} \lhd H^2F_{\tau_{,z}}F_{s_{,z}} \rhd_A \\
\\
K_{23}^{\tau sij} =& C_{22}\frac{1}{R}N_{i,\beta_{m2}} \lhd N_{m2}N_{n2} \rhd_\Omega N_{j_{n2}} \lhd H^2F_\tau F_s \rhd_A + C_{23}N_{i,\beta_{m2}} \lhd N_{m2}N_j \rhd_\Omega \lhd HF_\tau F_{s_{,z}} \rhd_A + \\
& C_{26}\frac{1}{R}N_{i,\alpha_{m3}} \lhd N_{m3}N_{n2} \rhd_\Omega N_{j_{n2}} \lhd H^2F_\tau F_s \rhd_A + C_{36}N_{i,\alpha_{m3}} \lhd N_{m3}N_j \rhd_\Omega \lhd HF_\tau F_{s_{,z}} \rhd_A + \\
& - C_{45}\frac{1}{R}N_{i_{m2}} \lhd N_{m2}N_{n1} \rhd_\Omega N_{j,\alpha_{n1}} \lhd F_\tau F_s \rhd_A - C_{44}\frac{1}{R}N_{i_{m2}} \lhd N_{m2}N_{n2} \rhd_\Omega N_{j,\beta_{n2}} \lhd F_\tau F_s \rhd_A + \\
& C_{45}N_{i_{m2}} \lhd N_{m2}N_{n1} \rhd_\Omega N_{j,\alpha_{n1}} \lhd HF_{\tau_{,z}}F_s \rhd_A + C_{44}N_{i_{m2}} \lhd N_{m2}N_{n2} \rhd_\Omega N_{j,\beta_{n2}} \lhd HF_{\tau_{,z}}F_s \rhd_A \\
\\
K_{31}^{\tau sij} =& C_{55}N_{i,\alpha_{m1}} \lhd N_{m1}N_{n1} \rhd_\Omega N_{j_{n1}} \lhd F_\tau F_{s_{,z}} \rhd_A + C_{45}N_{i,\beta_{m2}} \lhd N_{m2}N_{n1} \rhd_\Omega N_{j_{n1}} \lhd F_\tau F_{s_{,z}} \rhd_A + \\
& C_{12}\frac{1}{R}N_{i_{m2}} \lhd N_{m2}N_{n1} \rhd_\Omega N_{j,\alpha_{n1}} \lhd HF_\tau F_s \rhd_A + C_{13} \lhd N_iN_{n1} \rhd_\Omega N_{j,\alpha_{n1}} \lhd F_{\tau_{,z}}F_s \rhd_A + \\
& C_{26}\frac{1}{R}N_{i_{m2}} \lhd N_{m2}N_{n3} \rhd_\Omega N_{j,\beta_{n3}} \lhd HF_\tau F_s \rhd_A + C_{36} \lhd N_iN_{n3} \rhd_\Omega N_{j,\beta_{n3}} \lhd F_{\tau_{,z}}F_s \rhd_A \\
\\
K_{32}^{\tau sij} =& C_{22}\frac{1}{R}N_{i_{m2}} \lhd N_{m2}N_{n2} \rhd_\Omega N_{j,\beta_{n2}} \lhd H^2F_\tau F_s \rhd_A + C_{23} \lhd N_iN_{n2} \rhd_\Omega N_{j,\beta_{n2}} \lhd HF_{\tau_{,z}}F_s \rhd_A + \\
& C_{26}\frac{1}{R}N_{i_{m2}} \lhd N_{m2}N_{n3} \rhd_\Omega N_{j,\alpha_{n3}} \lhd H^2F_\tau F_s \rhd_A + C_{36} \lhd N_iN_{n3} \rhd_\Omega N_{j,\alpha_{n3}} \lhd HF_{\tau_{,z}}F_s \rhd_A + \\
& - C_{45}\frac{1}{R}N_{i,\alpha_{m1}} \lhd N_{m1}N_{n2} \rhd_\Omega N_{j_{n2}} \lhd F_\tau F_s \rhd_A - C_{44}\frac{1}{R}N_{i,\beta_{m2}} \lhd N_{m2}N_{n2} \rhd_\Omega N_{j_{n2}} \lhd F_\tau F_s \rhd_A + \\
& C_{45}N_{i,\alpha_{m1}} \lhd N_{m1}N_{n2} \rhd_\Omega N_{j_{n2}} \lhd HF_\tau F_{s_{,z}} \rhd_A + C_{44}N_{i,\beta_{m2}} \lhd N_{m2}N_{n2} \rhd_\Omega N_{j_{n2}} \lhd HF_\tau F_s \rhd_A \\
\\
K_{33}^{\tau sij} =& C_{22}\frac{1}{R^2}N_{i_{m2}} \lhd N_{m2}N_{n2} \rhd_\Omega N_{j_{n2}} \lhd H^2F_\tau F_s \rhd_A + C_{23}\frac{1}{R}N_{i_{m2}} \lhd N_{m2}N_j \rhd_\Omega \lhd HF_\tau F_{s_{,z}} \rhd_A + \\
& C_{23}\frac{1}{R} \lhd N_iN_{n2} \rhd_\Omega N_{j_{n2}} \lhd HF_{\tau_{,z}}F_s \rhd_A + C_{33} \lhd N_iN_j \rhd_\Omega \lhd F_{\tau_{,z}}F_{s_{,z}} \rhd_A + \\
& C_{55}N_{i,\alpha_{m1}} \lhd N_{m1}N_{n1} \rhd_\Omega N_{j,\alpha_{n1}} \lhd F_\tau F_s \rhd_A + C_{45}N_{i,\beta_{m2}} \lhd N_{m2}N_{n1} \rhd_\Omega N_{j,\alpha_{n1}} \lhd F_\tau F_s \rhd_A + \\
& C_{45}N_{i,\alpha_{m1}} \lhd N_{m1}N_{n2} \rhd_\Omega N_{j,\beta_{n2}} \lhd F_\tau F_s \rhd_A + C_{44}N_{i,\beta_{m2}} \lhd N_{m2}N_{n2} \rhd_\Omega N_{j,\beta_{n2}} \lhd F_\tau F_s \rhd_A
\end{aligned}
\tag{26}
$$

where $\lhd \ldots \rhd_\Omega$ indicates $\int_\Omega ...d\Omega$ and $\lhd \ldots \rhd_A$ indicates $\int_A ...dz$ (A is the integration domain in the z direction).

6 Numerical results

The model we have introduced, unlike 3-D degenerate approach, does not involve an approximation of the geometry of the shell and it describes accurately the curvature of the shell. However, the locking phenomenon is still present. In this work, such a model is combined with a simple displacement formulation. The high-order theories contained in CUF, coupled with the MITC method, allow us to increase the degree of approximation by increasing the order of expansion of displacements in the thickness direction and the number of used elements. We analyze the reliability of the model together with the finite element scheme, and we compare the numerical results with the ones obtained with the first order approximation (see [7]) and the ones obtained in the 3D degenerate approach (see [13]).
In this direction we consider two classical test problems. These problems are discriminating to test the performance of the finite elements. We consider the pinched cylinder with a diaphragm (Flügge, [26]) and the Scordelis-Lo problem (Scordelis and Lo, [27]). The pinched shell with a diaphragm is one of the most severe tests for both inextensional bending modes and complex membrane states. The Scordelis-Lo problem is extremely useful for determining the ability of an element to accurately solve complex states of membrane strain. A substantial part of the strain energy is membrane strain energy so the representation of inextensional bending modes is not crucial in this problem. We briefly describe each of the two test problems.

6.1 Pinched cylindrical shell

The first test we consider is the one called pinched shell. This structure has been analyzed in [7] and the essential shapes are shown in Fig. 3. The pinched shell is simply supported at each end by rigid diaphragm and singularly loaded by two opposed forces acting at midpoint of the shell. Due to the symmetry of the structure the computations have been performed, using a uniform decomposition, on a octave of the shell. Such a domain is described as:

$$S = \{(x, y, z) \in R^3 : \ 0 < x < L/2, \ 0 < y < R, \ y^2 + z^2 = R^2\} \tag{27}$$

corresponding to the rectangle:

$$\Omega = \{(\alpha, \beta) : \ 0 < \alpha < L/2, \ 0 < \beta < R\pi/2\} \tag{28}$$

The physical data given in Table 1 have been assumed. The following symmetry conditions are applied:

$$\begin{aligned} v_s(\alpha, 0) &= 0 \\ u_s(0, \beta) &= 0 \\ v_s(\alpha, R\pi/2) &= 0 \end{aligned} \tag{29}$$

and the following boundary conditions are prescribed:

$$v_s(L/2, \beta) = w_s(L/2, \beta) = 0 \tag{30}$$

with $s = 0, 1, ..., N$.

In Table 2 the transversal displacement at the loaded point C is presented for several decompositions $n \times n$ and different theories. The high-order equivalent single layer theories are indicated with the acronym ESLN, where N is the order of expansion. The exact solution is given by Flügge in [26] and it is 1.8248×10^{-5}[in]. The results (m) are obtained applying the MITC technique only to the membranal part of the in-plane strains (when τ or s is equal to 0), while the solution (m^+) is obtained for MITC applied to all terms of the expansion. In both cases, all terms of the expansion of the shear and normal strains are mixed interpolated. The figure 5 demonstrate that the two solutions in the Koiter case (as for the other theories) differs very little, especially when the number of elements is high (mesh 13×13). Therefore, we can refer always to (m^+) solution in the following analysis. The element shows good properties of convergence and robustness by increasing the mesh. According to Reddy [28] and Cho [29], the results obtained with high-order theories are grater than the reference value because Flügge refers to a classical shell theory. Indeed, the solution calculated with the Koiter model is very close to the exact solution for mesh 13×13, while the Naghdi model that takes into account the shear energy gives a higher value, as one can expect. The ESL theory with linear expansion (ESL1) produces such a high value because the correction of Poisson locking it has been applied (for details about Poisson locking one can refer to [30]), but in the case of cylindrical shell structures this correction gives some problems. The remaining theories provide almost the same results and they converge to the same value (1.842×10^{-5}[in]) by increasing the order of expansion and the number of used elements.

6.2 Scordelis-Lo problem

The problem deals with a cylindrical shell known in the literature as barrel vault. The shell is described in Fig.4. This typical shell is used in civil engineering using conventional processes by Scordelis and Lo [27]. The essential features of such example can be also found in [12]. The shell is simply-supported on diaphragms and is free on the other sides. The shell is loaded by its own weight P. The barrel vault is a portion of cylindrical shell, with midsurface described as follows:

$$S = \{(x, y, z) \in R^3 : \ -L/2 < x < L/2, \ -R\sin(2\pi/9) < y < R\sin(2\pi/9), \ z > 0 \ y^2 + z^2 = R^2\} \tag{31}$$

Applying the mapping (8) we get the following expression for Ω:

$$\Omega = \{(\alpha, \beta) : \ -L/2 < \alpha < L/2, \ -R2\pi/9 < \beta < R2\pi/9\} \tag{32}$$

The physical data given in Table 3 have been assumed.
The covariant components of the vertical load are: $p_1 = 0, \ p_2 = -P\sin(\beta/R), \ p_3 = P\cos(\beta/R)$.
The barrel vault has a symmetric structure. Thus, the computations have been performed only on a quarter of the shell, using a uniform decomposition. The following symmetry conditions have been assumed:

$$\begin{aligned} v_s(\alpha, 0) &= 0 \\ u_s(0, \beta) &= 0 \end{aligned} \tag{33}$$

and the following boundary conditions are prescribed:

$$v_s(L/2, \beta) = w_s(L/2, \beta) = 0 \tag{34}$$

with $s = 0, 1, ..., N$.

The exact solution for the present problem is given by McNeal and Harder in [31] in terms of transversal displacement at the point B and it is 0.3024[ft]. In Table 4 this quantity is calculated for several decompositions $n \times n$ and different theories. In this case, we provide only the (m^+) solution because the results obtained in the case (m) are very similar, also when a coarse mesh is considered. The table confirms the considerations done for the pinched shell: the results converge to the exact solution by increasing the order of expansion and the number of used elements. One can note that in this case the ESL1 theory doesn't give any problem because the shell is not cylindrical. Another difference regarding to the pinched shell is that the high-order theories and the classical theories provide almost the same results, because in this case we don't have local effects due to a concentrated load. In the Figures 6-8, for a given thickness of the shell, we compare the performance of the MITC9 element in which the correction of both shear and membrane locking has been applied (m^+), with the performance of the element in which only the shear locking has been corrected (s). For moderately thin shells $(t/R = 0.01)$ the correction of membrane locking is not so essential because for very fine mesh the two solutions converge. Instead, for very thin shells ($t/R = 0.001$ and $t/R = 0.0001$) the membrane locking phenomenon is remarkable and in this case one can note the high performances of the new element. We note that, as far as we know, the exact solution is not available for both cases $t/R = 0.001$ and $t/R = 0.0001$; however, our results show a qualitatively correct limit behavior for the solution (m^+) and we can conclude that MITC9 element is completely locking free. The theory used for this analysis is ESL4 but the behavior is the same also for the other models.

7 Concluding remarks

The aim of the present work is to present a shell finite element based on refined theories contained in CUF, in which the MITC technique has been applied to overcome the membrane and shear locking phenomenons. The results obtained by analyzing two classical test problems, such as pinched shell and Scordelis-Lo problem, show that:

- The MITC9 shell element presents good properties of convergence and robustness;
- The MITC method remains effective in the case of shell FEs formulated on the basis of higher-order theories contained in the Unified Formulation;
- The MITC9 element is completely locking free.

Future work could be directed towards the extension of MITC9 element to the analysis of multilayered structures as well as multi-field problems.

Acknowledgments

M Cinefra acknowledges the support of FNR of Luxembourg.

References

[1] W.T. Koiter, *"On the foundations of the linear theory of thin elastic shell."*, Proc. Kon. Nederl. Akad. Wetensch., 73, 169-195, 1970.

[2] P.M. Naghdi, *"The theory of shells and plates."*, Handbuch der Phisik, 6, 425-640, 1972.

[3] D.N. Arnold and R.S. Falk, *"A uniformly accurate finite element method for the Reissner-Mindlin plate."*, SIAM Journal of Numerical Analysis, 26, 1276-1290, 1989.

[4] J. Pitkäranta, *"The problem of membrane locking in finite element analysis of cylindrical shells."*, Numerische Mathematik, 61, 523-542, 1992.

[5] C. Chinosi, L. Della Croce and T. Scapolla, *"Numerical results on the locking for cylindrical shells."*, Computer-Assisted Mechanics and Engineering Sciences Journal, 5(1), 31-44, 1998.

[6] H. Hakula, Y. Leino and J. Pitkäranta, *"Scale resolution, locking, and higher-order finite element modelling of shells."*, Computer Methods in Applied Mechanics and Engineering, 133, 155-182, 1996.

[7] C. Chinosi, L. Della Croce and T. Scapolla, *"Hierarchic finite elements for thin Naghdi shell model."*, International Journal of Solids and Structures, 35, 1863-1880, 1998.

[8] 0.C. Zienkiewicz, R.L. Taylor and J.M. Too, *"Reduced integration techniques in general analysis of plates and shells."*, International Journal for Numerical Methods in Engineering, 3, 275-290, 1971.

[9] H. Stolarski and T. Belytschko, *"Reduced integration for shallow-shell facet elements."*, New Concepts in Finite Element Analysis, ed. by T.J.R. Hughes, et. al., ASME, New York, 179-194 (1981).

[10] J.J. Rhiu and S.W. Lee, *"A new effcient mixed formulation for thin shell finite element models."*, International Journal for Numerical Methods in Engineering, 24, 581-604, 1987.

[11] T.Y. Chang, A.F. Saleeb and W. Graf, *"On the mixed formulation of a nine-node Lagrange shell element."*, Computer Methods in Applied Mechanics and Engineering, 73, 259-281, 1989.

[12] K.-J. Bathe and E. Dvorkin, *"A formulation of general shell elements - the use of mixed interpolation of tensorial components."*, International Journal for Numerical Methods in Engineering, 22, 697-722, 1986.

[13] M.L. Bucalem and K.-J. Bathe, *"High-order MITC general shell elements."*, International Journal for Numerical Methods in Engineering, 36, 3729-3754, 1993.

[14] D.N. Arnold and F. Brezzi, *"Locking free finite element methods for shells."*, Methematics of Computation, 66, 1-14, 1997.

[15] C. Chinosi, L. Della Croce and T. Scapolla, *"Solving thin Naghdi shells with special finite elements."*, Mathematical Modelling and Scientific Computing, 8, 1997.

[16] E. Carrera, *"Theories and finite elements for multilayered plates and shells: a unified compact formulation with numerical assessment and benchmarking."*, Arch Comput Methods Eng, 97, 10-215, 2003.

[17] B. Brank and E. Carrera, *"Multilayered Shell Finite Element with Interlaminar Continuous Shear Stresses: A Refinement of the Reissner-Mindlin Formulation."*, International Journal for Numerical Methods in Engineering, 38, 843-874, 2000.

[18] E. Carrera, *"Multilayered Shell Theories that Account for a Layer-Wise Mixed Description. Part I. Governing Equations."*, AIAA Journal, 37, 1107-1116, 1999.

[19] E. Carrera, *"Multilayered Shell Theories that Account for a Layer-Wise Mixed Description. Part II. Numerical Evaluations."*, AIAA Journal, 37, 1117-1124, 1999.

[20] E. Carrera, *"A Study of Transverse Normal Stress Effects on Vibration of Multilayered Plates and Shells."*, Journal of sound and vibration, 225, 803-829, 1999.

[21] K.-J. Bathe, P.-S. Lee and J.-F. Hiller, *"Towards improving the MITC9 shell element."*, Computers and Structures, 81, 477-489, 2003.

[22] C. Chinosi and L. Della Croce, *"Mixed-interpolated elements for thin shell."*, Communications in Numerical Methods in Engineering, 14, 1155-1170, 1998.

[23] H.-C. Huang, *"Membrane locking and assumed strain shell elements."*, Compunters and Structures, 27(5), 671-677, 1987.

[24] P. Panasz and K. Wisniewski, *"Nine-node shell elements with 6 dofs/node based on two-level approximations. Part I Theory and linear tests."*, Finite Elements in Analysis and Design, 44, 784-796, 2008.

[25] D. Chapelle and K.-J. Bathe, *"The finite element analysis of shells.-Fundamentals."*, Springer, Berlin, 2003.

[26] W. Flügge, *"Stresses in shells."*, 2nd edn. Springer, Berlin, 1960.

[27] A. Scordelis and K.S. Lo, *"Computer analysis in cylindrical shells."*, Journal of American Concrete Institute, 61, 561-593, 1964.

[28] J.N. Reddy, *"Mechanics of laminated composite plates and shells. Theory and analysis."*, 2nd edn. CRC Press, Florida, 2003.

[29] M. Cho and H.Y. Roh, *"Development of geometrically exact new elements based on general curvilinear coordinates."*, International Journal for Numerical Methods in Engineering, 56, 81-115, 2003.

[30] E. Carrera and S. Brischetto, *"Analysis of thickness locking in classical, refined and mixed theories for layered shells."*, Composite Strcutures, 85(1), 83-90, 2008.

[31] R.H. McNeal and R.L. Harder, *"A proposed standard set of problems to test finite element accuracy."*, Finite elements in analysis and design, 1, 3-20, 1985.

Tables

Pinched shell		
Young's modulus	E	3×10^6 psi
Poisson's ratio	ν	0.3
load	P	1 lb
length	L	600 in
radius	R	300 in
thickness	t	3 in

Table 1: Physical data for pinched shell.

Theory	$[4 \times 4]m$	$[4 \times 4]m^+$	$[10 \times 10]m$	$[10 \times 10]m^+$	$[13 \times 13]m$	$[13 \times 13]m^+$
Koiter	1.7733	1.7891	1.8189	1.8231	1.8227	1.8253
Naghdi	1.7827	1.7984	1.8323	1.8364	1.8372	1.8398
ESL1	1.9048	1.9212	1.9541	1.9583	1.9591	1.9617
ESL2	1.7663	1.7805	1.8322	1.8361	1.8383	1.8408
ESL3	1.7676	1.7818	1.8341	1.8380	1.8404	1.8428
ESL4	1.7676	1.7818	1.8341	1.8380	1.8404	1.8428

Table 2: Pinched shell. Transversal displacement w[in]$\times 10^5$ at the loaded point C of the mid-surface S.(exact solution: 1.8248×10^{-5}[in])

Barrel vault		
Young's modulus	E	4.32×10^8 lb/ft^2
Poisson's ratio	ν	0.0
load	P	90 lb/ft^2
length	L	50 ft
radius	R	25 ft
thickness	t	0.25 ft
angle	θ_0	$2\pi/9$ rad

Table 3: Physical data for barrel vault.

Theory	$[4 \times 4]m^+$	$[10 \times 10]m^+$	$[13 \times 13]m^+$
Koiter	0.2953	0.3015	0.3025
Naghdi	0.2954	0.3018	0.3029
ESL1	0.2954	0.3018	0.3029
ESL2	0.2954	0.3018	0.3029
ESL3	0.2954	0.3019	0.3029
ESL4	0.2954	0.3019	0.3029

Table 4: Barrel vault. Transversal displacement w[ft] at the point B of the midsurface S.(exact solution: 0.3024[ft])

Figures

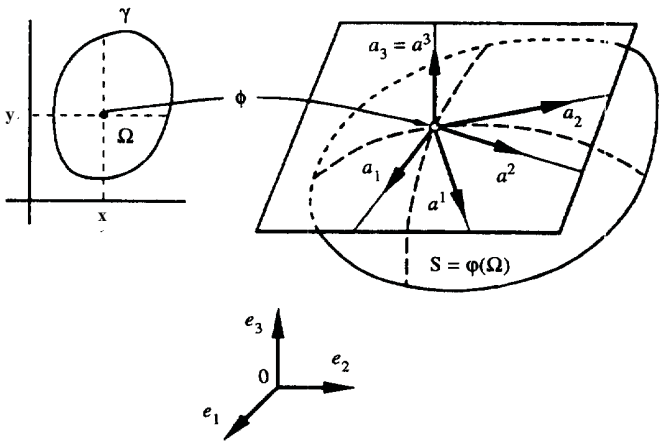

Figure 1: Definition of the middle surface.

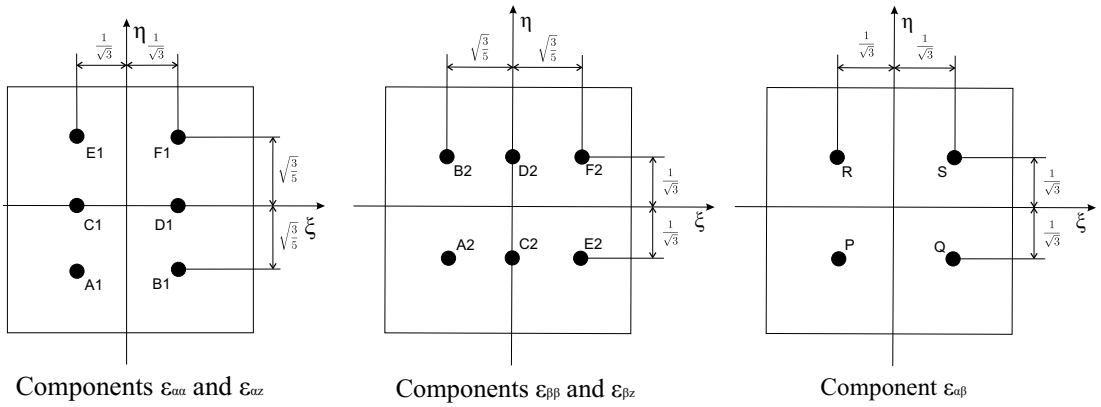

Figure 2: Tying points for MITC9 shell finite element.

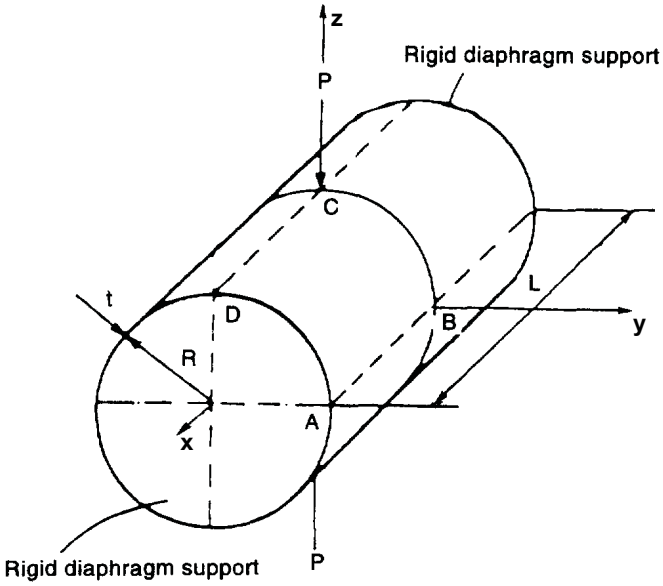

Figure 3: Pinched shell.

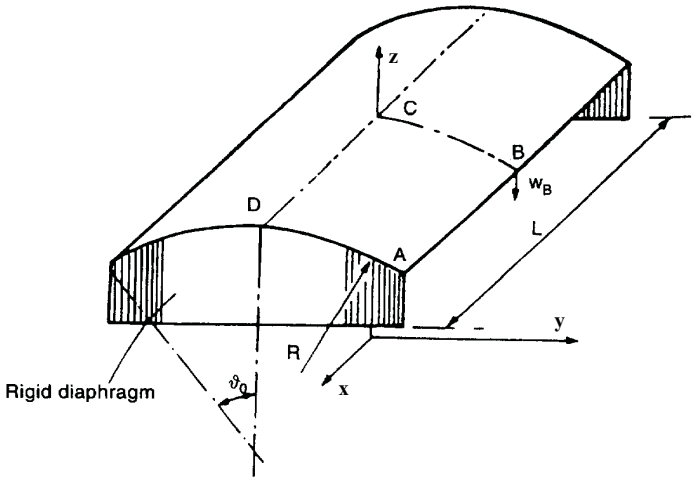

Figure 4: Scordelis-Lo roof.

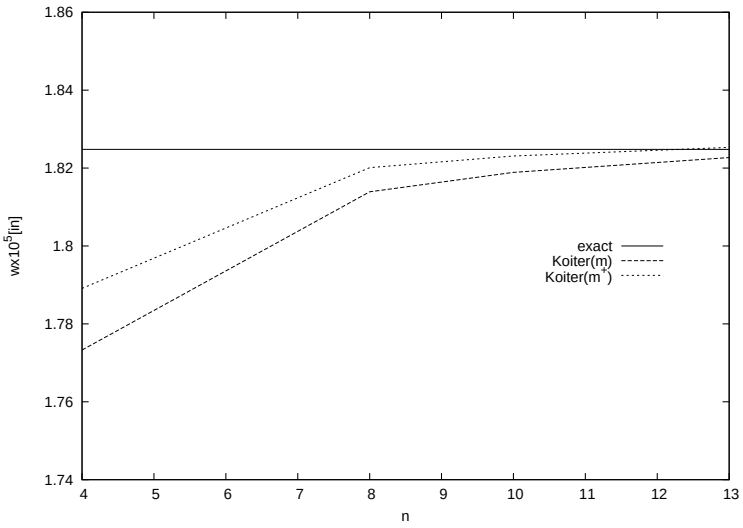

Figure 5: Pinched shell. Transversal displacement $w[\text{in}]\times 10^5$ at the loaded point C of the midsurface S by varying the mesh $n \times n$.

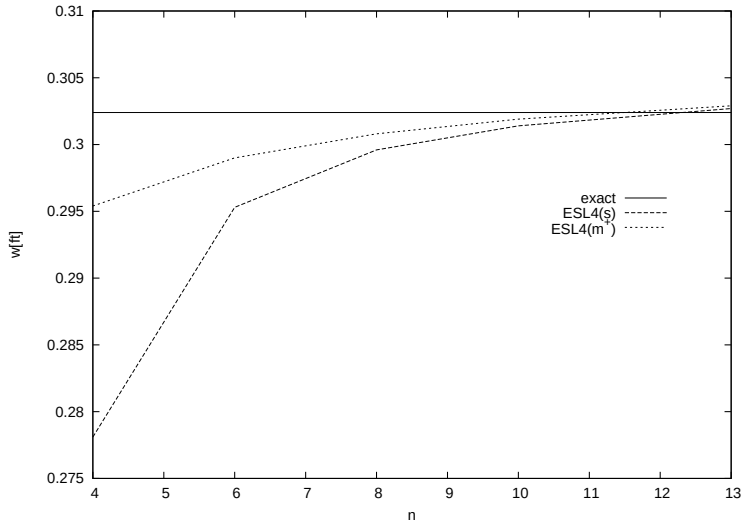

Figure 6: Scordelis-Lo problem. Thickness ratio $t/R = 0.01$. Transversal displacement w[ft] at the point B of the midsurface S by varying the mesh $n \times n$.

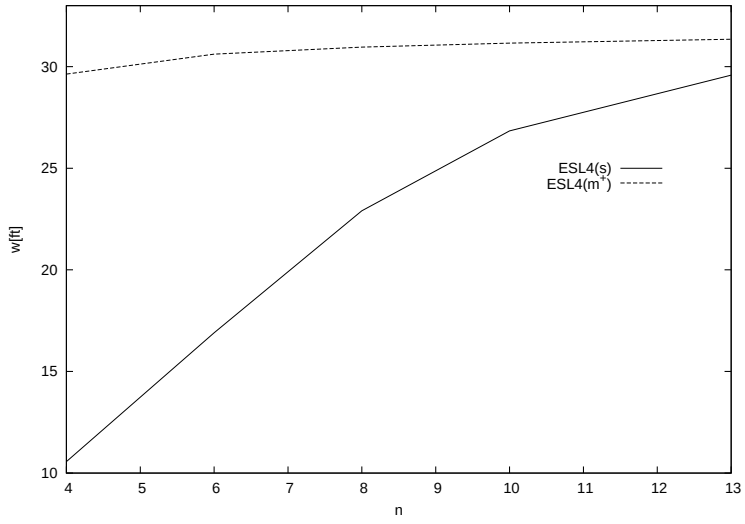

Figure 7: Scordelis-Lo problem. Thickness ratio $t/R = 0.001$. Transversal displacement w[ft] at the point B of the midsurface S by varying the mesh $n \times n$.

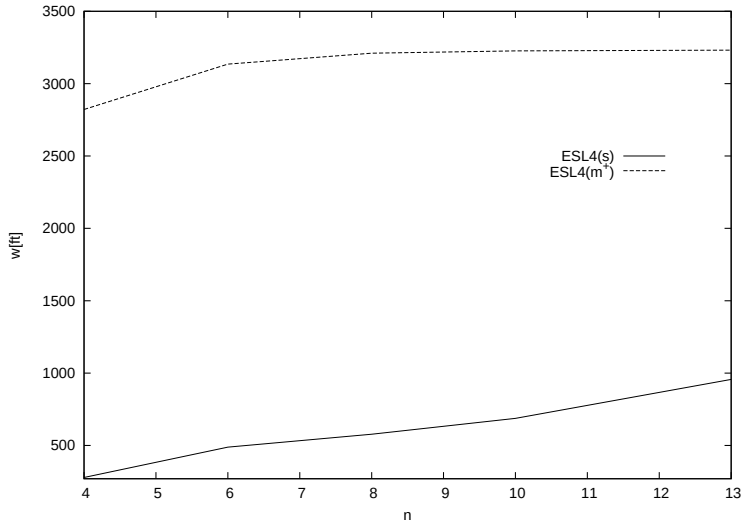

Figure 8: Scordelis-Lo problem. Thickness ratio $t/R = 0.0001$. Transversal displacement w[ft] at the point B of the midsurface S by varying the mesh $n \times n$.